Minimizing Height Effects in MTInSAR for Deformation Detection Over Built Areas

Lei Zhang, *Senior Member, IEEE*, Hongguo Jia, Zhong Lu, Hongyu Liang, *Student Member, IEEE*, Xiaoli Ding, and Xin Li

***Abstract*— Removing the topographic component in the interferometric synthetic aperture radar (InSAR) phase is conventionally conducted using an external digital elevation model (DEM). However, with an increasing spatial resolution of SAR data, the external DEM is becoming less qualified for this purpose, resulting in notable phase residues and even decorrelation in differential interferograms. Although topographic residuals can be parameterized and estimated by multi-temporal InSAR (MTInSAR) techniques, its accuracy is limited by several factors. Instead of providing accurate height information, shortening the length of baselines is an alternative for DEM phase mitigation. We propose here an MTInSAR processing framework that can retrieve the deformation time series without the estimation of topographic residuals. Within the framework, we generate a set of pseudo interferograms with near-zero baselines by integer combination and take these pseudo interferograms as observations of MTInSAR model, where deformation becomes the only signal that needs to be parameterized. The deformation time series is then retrieved directly from wrapped phases by ridge estimation with an integer ambiguity detector. It is noted that although atmospheric artifacts might be magnified during the combination, their differential components at arcs constructed with neighboring points that are not significantly enlarged. The proposed method is particularly suitable for infrastructure deformation monitoring in urban areas where no accurate external DEM is available. It also has promising potential for retrieving deformation from SAR data stacks with short acquisition intervals since the combination can enlarge the signal of interests in pseudo-observations. Semisynthetic and real data tests indicate that the proposed method has satisfied performance on DEM error mitigation and deformation time series estimation.**

***Index Terms*— Deformation time series, integer combination, interferometric synthetic aperture radar (InSAR), ridge estimation.**

I. Introduction

InSAR has greatly advanced the capability of monitoring ground deformation [1]–[7] because of its unique features of all-weather and day-and-night imaging capability, global coverage, remote observation, fine resolution, and high accuracy. Such a capability will be further enhanced by future SAR missions (e.g., Tandem-L [8]). Since InSAR measurement is a mixture of phase components mainly associated with topography and deformation, when deformation is a signal of interest, it is necessary to mitigate the topographic contribution. To attain this purpose, differential operation with an external digital elevation model (DEM) is conventionally conducted [9]. However topographic residuals always exist in differential interferograms, especially those with long perpendicular baselines due to the limited accuracy of existing external DEMs (e.g., Shuttle Radar Topography Mission (SRTM) DEM [10]) [11]. With the development of modern SAR sensors, the spatial resolution of SAR images has been notably improved, thereby raising more challenges for external DEMs to mitigate the topographic component in InSAR measurements. Even with the release of the latest global DEM with a spatial resolution of 12 m [12], it is still not sufficient for such a purpose. Strictly speaking, there is no perfect external DEM for differential operation considering the discrepancy between the location of backscattering point and target height. Moreover, rapid urbanization, especially in developing countries, is changing landscapes significantly with the DEM usually updated less frequently, resulting in phase residuals in differential InSAR processing. For example, Fig. 1 shows a 3-m differential TerraSAR-X interferograms over buildings in Tianjin, China, where the SRTM DEM with a resolution of 90 and 30 m is used. A notable height phase residual is visible due to the inaccurate and outdated external DEM and relatively long perpendicular baseline.

As there is a direct relationship between the phase residual and the DEM error, the DEM error is usually taken as a parameter in the multi-temporal InSAR (MTInSAR) techniques (e.g., Persistent Scatterer Interferometry (PSI) [13], Small BAseline Subset (SBAS) [14], Multidimensional SBAS (MSBAS) [15], Coherent Pixel Technique (CPT) [16], temporarily coherent point SAR interferometry (TCPInSAR) [17], [18], Component extrAction and sElection SAR (CAESAR) [19], Parisar [20]). Indeed, with an ideal distribution of perpendicular baselines and the assumption that

Manuscript received October 5, 2018; revised March 7, 2019 and May 3, 2019; accepted May 17, 2019. This work was supported in part by the National Nature Science Foundation of China under Grant 41774023, Grant 41304011, and Grant 41701535, in part by the Research Grants Council of Hong Kong under Grant PolyU 152232/17E, and in part by the Sichuan Science and Technology Program under Grant 2019YJ0224. *(Corresponding author: Hongguo Jia.)*

L. Zhang was with the Department of Land Surveying and Geo-Informatics, The Hong Kong Polytechnic University, Hong Kong. He is now with the Faculty of Architecture, The University of Hong Kong, Hong Kong (e-mail: lslzhang@hku.hk).

X. Ding, H. Liang, and X. Li are with the Department of Land Surveying and Geo-Informatics, The Hong Kong Polytechnic University, Hong Kong (e-mail: allenhongyu.liang@connect.polyu.hk; xl.ding@polyu.eud.hk; vivianyoxi@gmail.com).

H. Jia is with the Faculty of Geosciences and Environmental Engineering, Southwest Jiaotong University, Chengdu 611756, China (e-mail: rsJia@swjtu.edu.cn).

Z. Lu is with the Roy M. Huffington Department of Earth Sciences, Southern Methodist University, Dallas, TX 75275 USA (e-mail: zhonglu@smu.edu).

Color versions of one or more of the figures in this paper are available online at http://ieeexplore.ieee.org.

Digital Object Identifier 10.1109/TGRS.2019.2925115

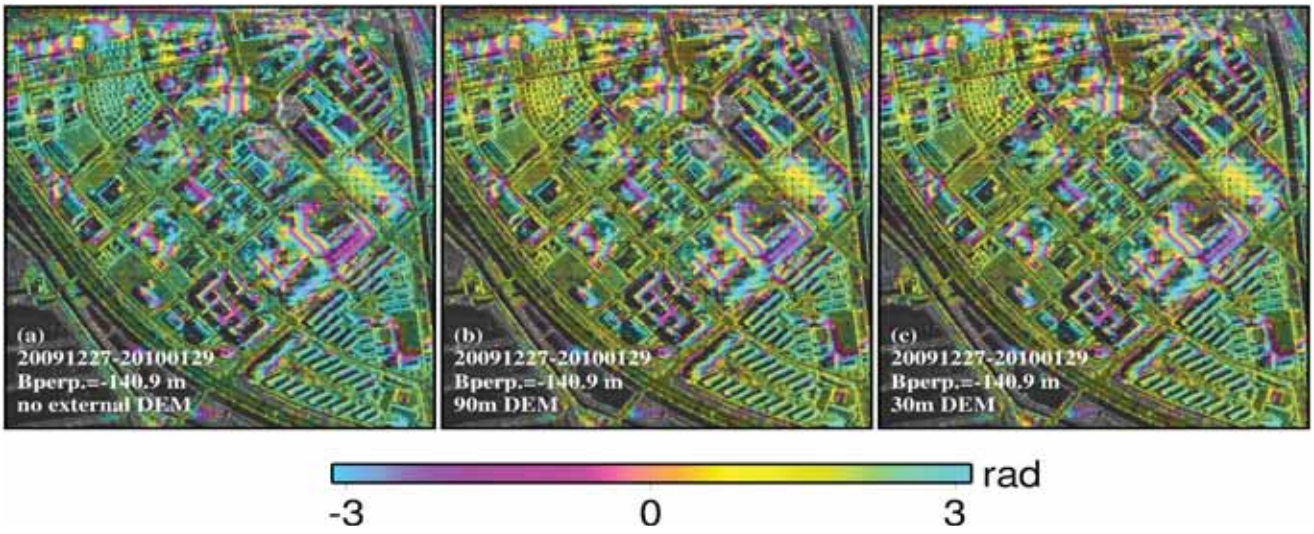

Fig. 1. Interferograms illustrating differential operation with external DEMs might not be sufficient for DEM mitigation. (a) Original interferogram. (b) Differential with 90-m SRTM DEM. (c) Differential with 30-m SRTM DEM. There is no difference between the corrected interferograms because the buildings were constructed after the SRTM DEM mission.

the parameters can well describe the real deformation (i.e., model bias is neglectable), both displacement and height on coherent targets can be satisfactorily estimated. However, the performance of current MTInSAR techniques on the joint estimation of DEM error and deformation can be affected by several factors, e.g., the deformation model, the connectivity of interferogram network, and the baseline variation and threshold [21]. Considering that current satellite SAR systems usually prefer a narrow baseline tube (e.g., Sentinel-1A/B), conventional MTInSAR algorithms might not guarantee an accurate estimation of heights from the data acquired by these sensors. The remaining DEM residuals can distort the estimation of deformation time series [21]. This was also pointed out by Bayer *et al.* [22] who explored how InSAR results vary with choices of the external DEM based on two popular MTInSAR models (i.e., PSI and SBAS) and concluded that the DEM quality is more important than the resolution and that X-band InSAR data are more sensitive to the choice of the DEM than C-band.

Since the current MTInSAR models cannot reliably ensure a qualified estimation of DEM errors, an alternative is to mitigate the DEM effect instead of estimating it directly. Such an idea arose from the fact that the phase contribution of DEM in InSAR measurements is determined by both the topographic height and perpendicular baseline. If only the interferograms with extremely short baselines are involved in the processing chain, since the DEM related phase is quite subtle and can be safely ignored, the deformation vector will then become the only unknowns in the MTInSAR model. Interferograms generated by modern satellite radars (e.g., TerraSAR-X and Sentinel-1A/B) can repeat the trajectory much better than previous ones [23], [24] that usually have short baselines, thanks to excellent control of satellite and orbit determination. However, the number of such small-baseline interferograms can never be guaranteed.

To achieve sufficient interferometric pairs with rather short baselines, we attempt here to adopt an integer combination strategy to generate pseudo-interferograms, which will be taken as observations of MTInSAR model. Integer combination of interferograms was first proposed in [25] and then in [26] for reducing phase fringes and therefore easing or avoiding phase unwrapping. Later, the strategy was also used to process the European Remote Sensing Satellite (ERS)/ENVISAT cross-platform interferograms where the topography-induced fringes are very dense due to the very long baselines (usually longer than 2 km) [27]. It is worth noting that besides reducing the fringes contributed by topographic heights, integer combination is also capable of increasing the signal of deformation as the temporal interval can be enlarged. Considering the repeat cycle of modern sensors is getting shorter and shorter (e.g., 1 d for COSMO-SkyMed constellation), the combined interferograms are more helpful for retrieving weak but time-dependent movements (e.g., postseismic motion). From the pseudo-interferograms, we then isolate coherent points, construct dense arcs (i.e., point pairs) and build up the relationship between the deformation parameters and differential pseudo-phases at arcs. Considering the correlation among the deformation rates in successive acquisition intervals, a ridge estimator with an ability of phase ambiguity detection is employed to retrieve these parameters. Finally, the deformation time series is obtained by integrating the relative deformation rate vector at arcs with respect to a reference point and accumulating the interval deformations to a reference acquisition date. Since the proposed method can retrieve the deformation from InSAR measurements without estimation of target heights, it is suitable for surveillance of abnormal deformation over large-scale urban areas, while, when monitoring single structures, accurate height information is still compulsory as the geolocation of coherent targets is crucial.

The rest of the paper is organized as follows: Section II introduces the principle of integer combination and the MTInSAR model based on the pseudo-interferograms with near-zero baselines. In Section III, synthetic and real data tests are described, which are used to validate and demonstrate the performance of the proposed strategy. Section IV provides conclusions and suggestions.

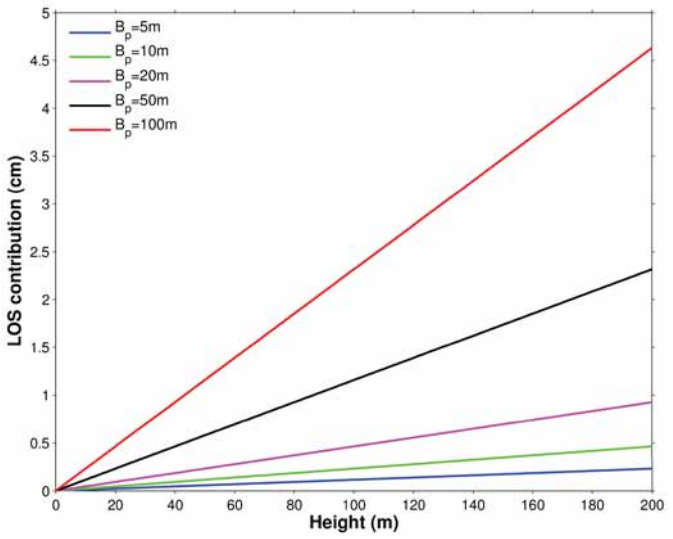

Fig. 2. Contribution of height to the LOS range change under different perpendicular baselines.

II. Methodology

A. Topographic Phase

The topographic phase that reflects the phase contribution of heights can be expressed as [28]

$$\phi_{\mathrm{h}} = -\frac{4\pi}{\lambda}\frac{B_{\perp} h}{\rho \sin\theta} \tag{1}$$

where λ is the wavelength of radar pulse; ρ is the slant range from sensor to the ground target; θ is the incidence angle; $B_{\perp}$ is the perpendicular spatial baseline, and h is the target height. It is clear that under a fixed imaging geometry, the phase contribution of height at a certain target is proportional to the perpendicular baseline. The slant range contribution (SRC, Δl) of topographic phase can then be further derived as

$$\Delta l = \frac{B_{\perp} h}{\rho \sin\theta}. \tag{2}$$

It has no relation with radar wavelength. Fig. 2 shows the SRC under different combinations of perpendicular baseline and heights, where the slant range and incidence angle are extracted from TerraSAR-X data (i.e., 657 330 m and 41, respectively). If the perpendicular baseline is short enough, the SRC will be negligible. Considering the primary application of the proposed processing strategy is infrastructure monitoring in urban areas where abundant persistent scatterers can be identified, the height difference [or height residual difference, after Differential SAR Interferometry (DInSAR) operation] between most neighboring scatterers should be within several tens of meters. When limiting the baseline of pseudo-interferograms to 5 m, it is safe to ignore the contribution of heights on SRC at most arcs.

B. Integer Combination

Given N single look complex (SLC) images coregistered to the same imaging geometry, a total of $N(N-1)/2$ interferograms can be generated. For persistent scatterers, all the interferograms could be taken as the observations of MTInSAR processing while, for distributed scatterers, only a portion of them having relatively smaller baselines can be used. To balance the spatial density of the selected points and phase noise, we use M interferograms in the proposed processing chain. For the pseudo interferometric phase (ϕ_{pseudo}) constructed from original interferograms (ϕ_n and ϕ_m), following the law of error propagation, the noise of combined interferograms (σ_{pseudo}) can be obtained as

$$\begin{aligned} \phi_{\mathrm{pseudo}} &= a \cdot \phi_n + b \cdot \phi_m \\ \sigma^2_{\mathrm{pseudo}} &= a^2 \cdot \sigma_n^2 + b^2 \cdot \sigma_m^2 + 2ab \cdot \sigma^2_{\mathrm{nm}} \end{aligned} \tag{3}$$

where a and b are combination integers; σ_n and σ_m represent the noise of the original interferograms; σ^2_{nm} is the covariance of the two interferograms involved. If these two interferograms share a common image or if the images were acquired under similar conditions, their corresponding σ^2_{nm} is nonzero and can be calculated following the strategy described in [29]. It is worth noting that (3) is suitable for the processing noise (e.g., errors introduced by filtering and multi-looking operations), while not for decorrelation noise that is not temporarily random. To control the noise level, we limit the combination integers to ± 1 and ± 2. To generate pseudo-interferograms with ultrashort baselines, a combination searching is conducted over the selected interferograms. The possible combinations are first determined according to the integer numbers, where those resulting in the same absolute pseudo perpendicular baselines are deleted, then the iterative calculation is conducted for the baseline vector of selected interferograms, and finally, the combinations whose baselines are less than the threshold are selected. When a total of K pseudo-interferograms are generated, the relationship between combined interferograms (Φ_{pseudo}) and original ones (Φ^{ori}) is expressed as

$$\Phi_{\mathrm{pseudo}} = W\{C\Phi^{\mathrm{ori}}\} \tag{4}$$

where $W\{\cdot\}$ is the wrapping operator and C is the combination matrix with a size of $K \times M$ whose elements are 0, ± 1, and ± 2. Fig. 3(a) and (b) shows an example combination of two TerraSAR-X interferograms. After their perpendicular baselines were shortened from over 140 m to less than 1 m in the pseudo-interferogram, the height fringes become invisible [Fig. 3(c)]. Fringe reduction is notable as seen from the phase profiles [Fig. 3(d)].

C. MTInSAR Modeling and Parameter Estimation

In the pseudo-interferograms, the topographic contribution is insignificant due to the ultrashort baselines; therefore, only the displacement parameters need to be modeled. To enhance the estimation stability especially in the case where the interferogram network has subsets (i.e., the normal matrix of the MTInSAR model is rank-deficiency), we adopt here the deformation rate in ordered acquisition intervals as parameters. Similar strategies were also adopted in [14], [30], and [31]. For a given (ith) pseudo-interferogram, the phase can then be modeled as

$$\begin{aligned} \phi_i^{\mathrm{pseudo}} &= W\left\{-\frac{4\pi}{\lambda}\sum_{j=1}^{2} n_j \phi_j\right\} \\ &= W\left\{-\frac{4\pi}{\lambda}\left(n_1 \sum t_m \cdot v_m + n_2 \sum t_p \cdot v_p\right)\right\} \end{aligned} \tag{5}$$

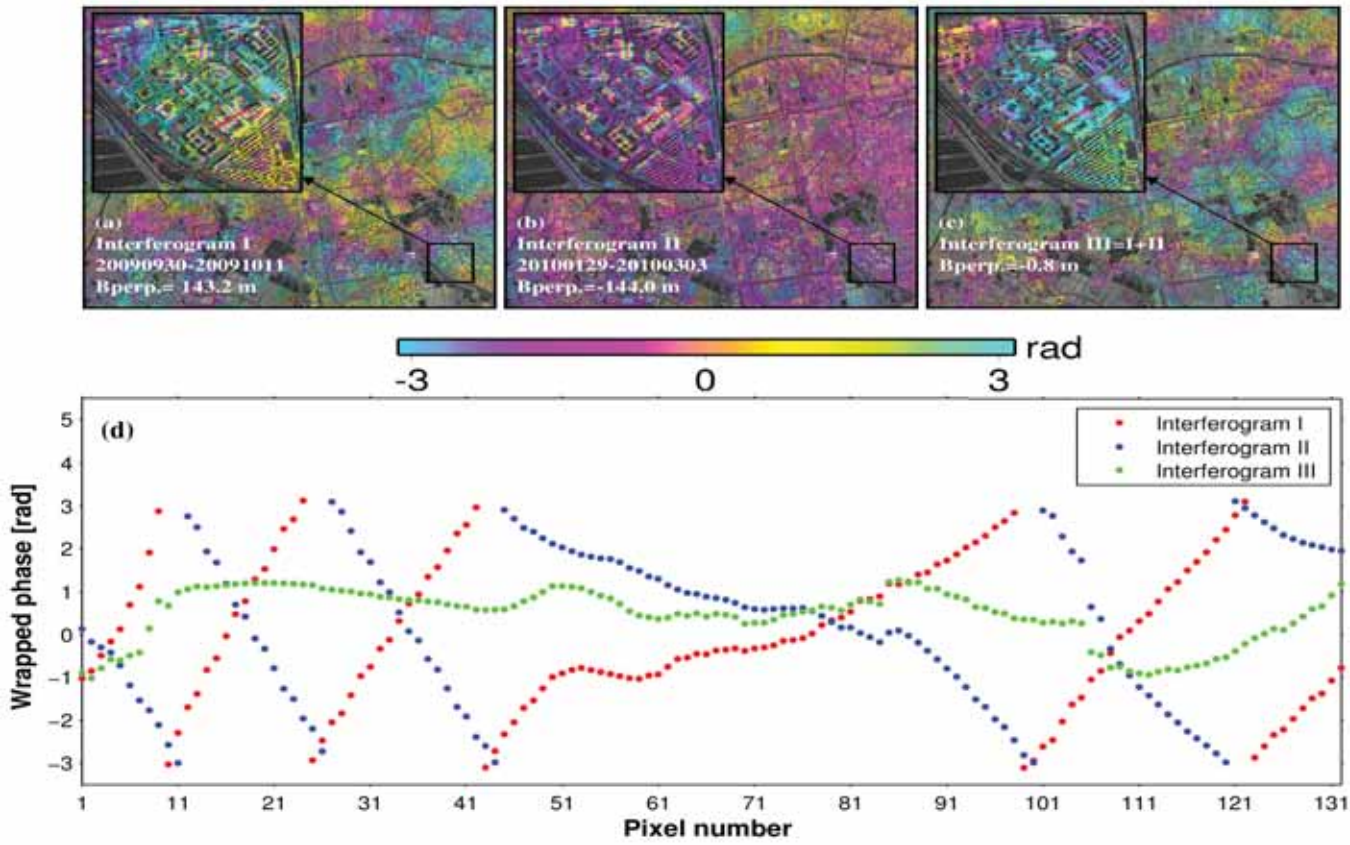

Fig. 3. Example of integer combination of interferograms. (a) Original interferogram I with a baseline of 143.2 m. (b) Original interferogram II with a baseline of −144.0 m. (c) Combined interferogram with integers of 1 and 1. Its baseline was reduced to −0.8m. (d) Phase profiles along the red lines in the interferograms.

where n_j is an integer indicating the magnified contribution of the deformation in that interval; m and p indicate the time intervals involved in the original interferograms that are used for the combination pseudo-interferogram; t_m and t_p are the time spans in the intervals of m and p; v_m and v_p are the unknowns, which could be the same since the two original interferograms can have overlapped intervals. Considering an arc constructed by two neighboring (not necessarily the nearest) coherent points, the phase difference can be modeled accordingly, as follows:

$$\phi_{i,\,\mathrm{arc}}^{\mathrm{pseudo}} = W\left\{-\frac{4\pi}{\lambda}(n_1\sum t_m\cdot\Delta v_m + n_2\sum t_p\cdot\Delta v_p)\right\} \quad (6)$$

where Δv is the relative deformation rate between these two points, which will be transferred to the rates at points by spatial integration. For each arc, the observation function reflecting the relationship between phase differences and relative deformation rates can be expressed in the matrix as

$$\mathbf{\Phi}^{\mathrm{pseudo}} = \mathbf{AV} \quad (7)$$

where $\mathbf{A}$ is the design matrix, including elements determined by combination integers and temporal intervals and unknowns; $\mathbf{V}$ contains the relative deformation rates in successive intervals. It should be noted that the observations in (7) are wrapped phases and the observation system is not rank-deficiency if the interferogram network has no subset.

D. Parameter Estimation and Atmospheric Artifacts Suppression

For retrieval of parameters from wrapped phases, solution space searching is a widely adopted method, where a searching interval for each parameter is predefined. However, considering that the parameters here are the relative deformation rates in successive intervals whose number equals $N-1$, it is very difficult, if not impossible, to achieve a reliable estimation via searching. As an alternative, we adopt here the strategy proposed in [17] and [18] to estimate the parameters, whereby the phase ambiguities in the wrapped phases are designated as outliers since they can result in abnormally large residuals when conducting least squares directly on (7) [17]. By simply comparing the maximum absolute residual with a predefined threshold, arcs having observations with nonzero integer ambiguity can be detected and removed. However, since the proposed model uses the deformation rates in ordered intervals as parameters, it has a risk of over-parameterization and, therefore, possibly makes the observation function ill-posed. For example, over an area undergoing linear subsidence where the interval rates meet $v_1 = v_2 = \cdots = v_{N-1} = v$, for any given arc, when the rate vector $[v_1\ v_2\ \cdots\ v_{N-1}]^T$ is unknown, the observation system is obviously over-parameterized and the coefficient matrix of a normal function (i.e., $\mathbf{A}^T\mathbf{A}$, if weight matrix is ignored) is ill-posed, leading to an unstable estimation

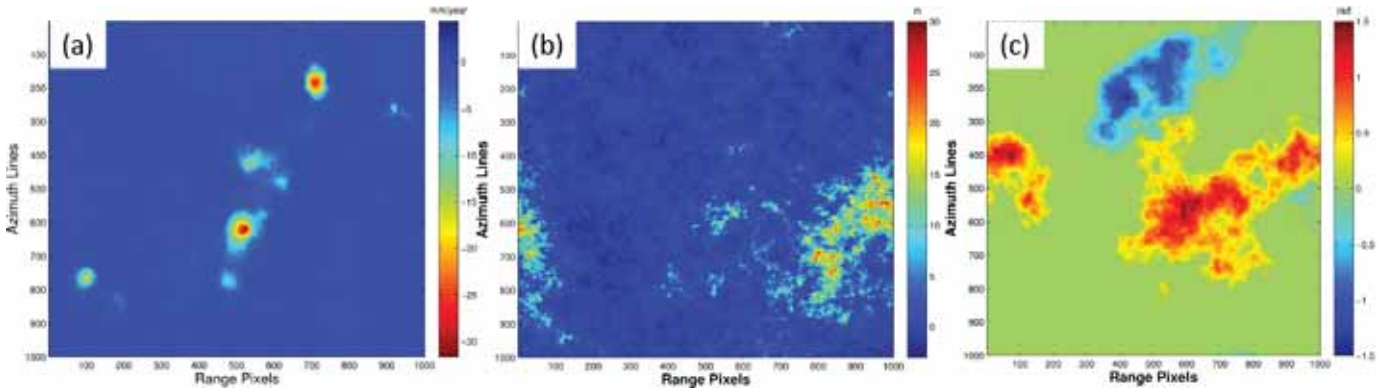

Fig. 4. Simulated signals for assessing the performance of the proposed method. (a) Deformation rate map. (b) DEM residuals. (c) Atmospheric artifacts associated with a certain acquisition date.

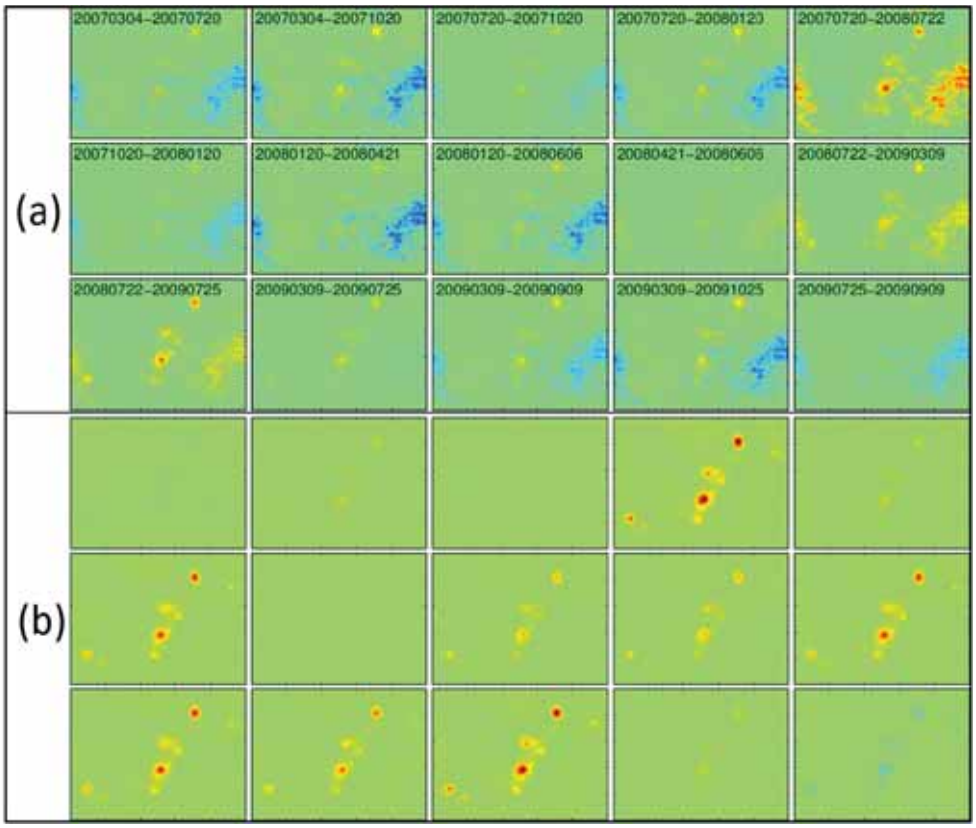

Fig. 5. (a) Simulated interferograms where only the deformation, DEM error, and noise are considered. (b) Pseudo-interferograms combined with integers from the original ones.

of parameters. To overcome this, Tikhonov regularization is commonly used [32], [33], which is also known as ridge regression in statistics. The regularization solves (7) with the following minimization:

$$\min_v (\|\mathbf{\Phi}^{\text{pseudo}} - \mathbf{AV}\| + k\|\mathbf{V}\|^2) \tag{8}$$

where $k > 0$ is the regularization parameter. Several methods are available for determination of its value, e.g., discrepancy principle, general cross-validation, L-curve [34]. The corresponding solution is then derived as

$$\begin{aligned} \hat{V} &= (\mathbf{A}^T\mathbf{WA} + k\mathbf{I})^{-1}\mathbf{A}^T\mathbf{W}\mathbf{\Phi}^{\text{pseudo}} \\ \mathbf{e} &= (\mathbf{I} - \mathbf{A}(\mathbf{A}^T\mathbf{WA} + k\mathbf{I})^{-1}\mathbf{A}^T\mathbf{W})\mathbf{\Phi}^{\text{pseudo}} \end{aligned} \tag{9}$$

where $\mathbf{W}$ is the positive-definite weight matrix whose elements can be determined by the mean coherence of two points involved in the given arc and $\mathbf{e}$ is the residual of ridge regression. For each arc, the maximum absolute residual will be compared with a given threshold to determine whether the differential phase at the arc contains phase ambiguity. Considering that the main application scenario of the proposed processing method focuses on urban areas where dense fringes contributed by building heights commonly exist in differential interferograms, the combination can significantly reduce the phase ambiguities in pseudo-interferograms and therefore ease the phase ambiguity detection and improve the estimation reliability. Moreover, since the parameter estimation is directly

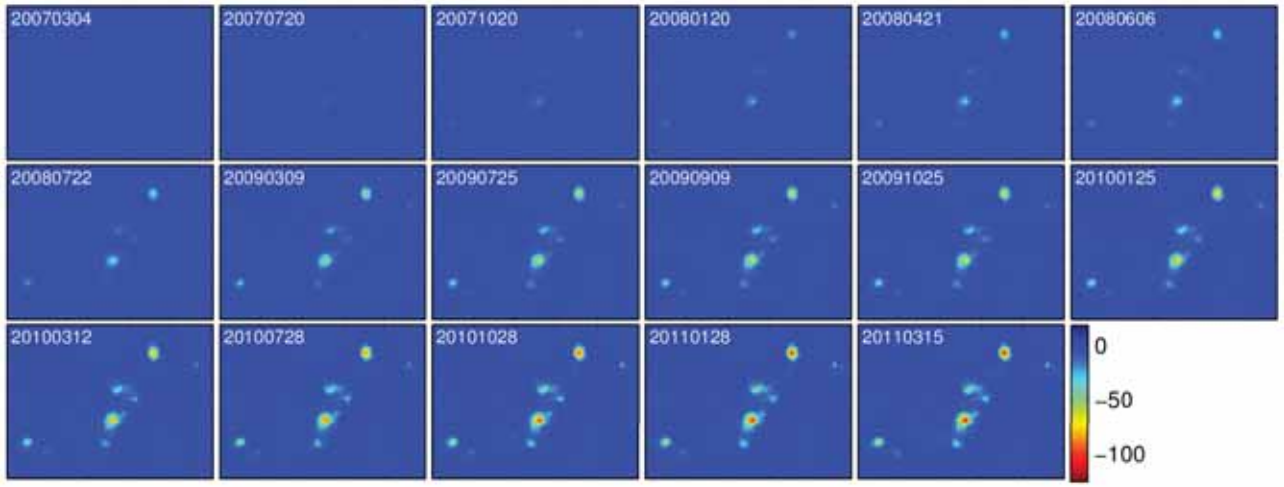

Fig. 6. Deformation time series estimated from the pseudo-observations with the proposed method.

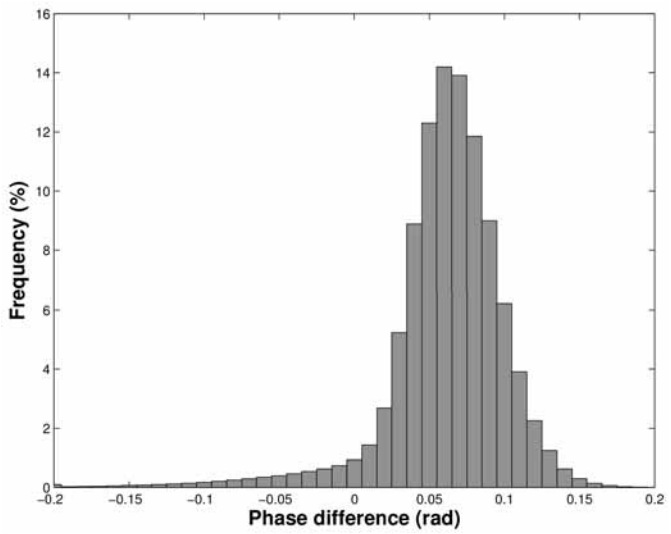

Fig. 7. Histogram of differences of absolute atmospheric phases at arcs in original and combined interferograms.

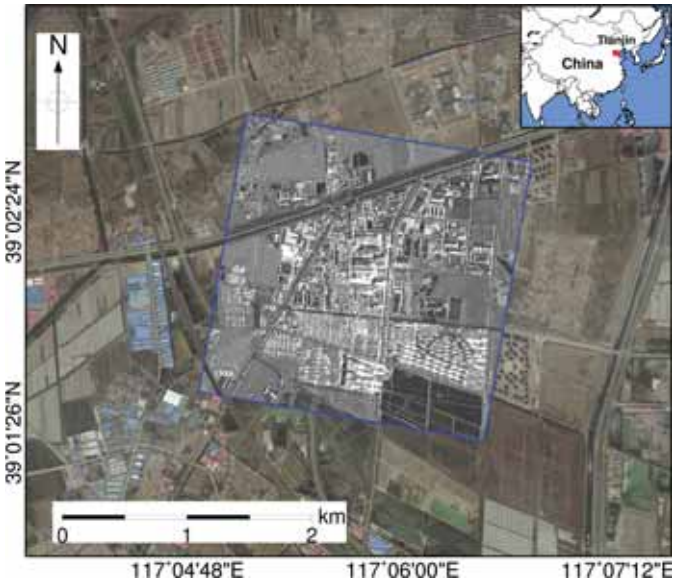

Fig. 8. Location of the testing site over an urbanized area of Tianjin, China, where the SAR intensity image was superimposed on Google satellite image.

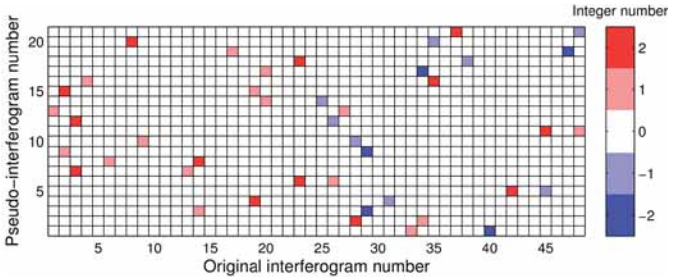

Fig. 9. Integer combination matrix.

conducted at densely constructed arcs (i.e., point pairs), differential operation between neighboring points can reduce a large portion of atmospheric delay [35], and therefore, this side-effect of combination is tolerable. Even in the extreme cases where the enlarged atmospheric delay introduced phase ambiguity to some arcs, these arcs can be detected and removed by determining their estimation residuals. However, it is worth noting that the aforementioned operation cannot completely mitigate the effects of atmospheric artifacts on parameter estimation, and postprocessing (e.g., spatial-temporal filtering) is usually compulsory.

After the estimation, the parameters at remained arcs are then transferred to points by spatial integration with respect to a reference point, according to the following:

$$\mathbf{V}_{\text{arc}} = \mathbf{B}\mathbf{V}_{\text{point}} \tag{10}$$

where $\mathbf{B}$ is a linking matrix having a size of L by $P-1$ (L and P are the number of remained arcs and points, respectively). It only contains elements of 0, 1, and -1. Considering that the noise level of arcs varies from one to another, optimization of integration network based on the abundant arcs could also be adopted [36].

III. Semisynthetic and Real Data Tests

To assess the performance of the proposed modeling strategy, we simulate a set of interferograms based on the

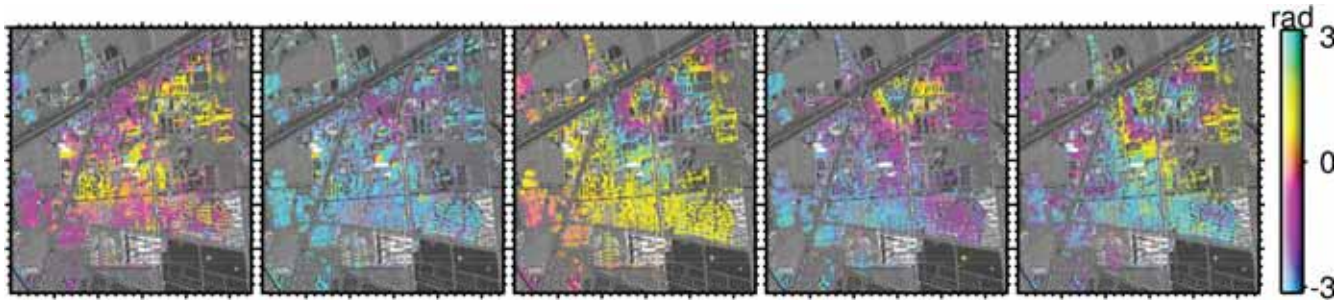

Fig. 10. Examples of original (the first two) and combined interferograms (the last three) whose perpendicular baselines are −220, 186, 0.1, 0.3, and 0.7 m, respectively.

spatial-temporal baselines of real ALOS/PALSAR interferometric pairs where the phase components related to the topographic errors, ground deformation, and noise are considered. The atmospheric artifacts simulated according to [28] are also added. The spatial pattern of some components is shown in Fig. 4. A total of 27 interferograms are generated from 17 radar images, whose absolute perpendicular baselines vary from 56 to 803 m. They serve as basic observations of the proposed model. Combination searching is then conducted to construct the ultrashort baseline pseudo interferograms. With a combined baseline threshold of 20 m, there are 23 pseudo interferograms selected, from which the deformation time series can be estimated. As a comparison, Fig. 5 shows some examples of original and pseudo interferograms. It is clear that the topography-raised phase component has been notably reduced and is virtually invisible in the pseudo interferograms. Even though the input deformation signal is linear, we model it here with an interval rate vector. The purpose of such an operation is to enhance the generality of our proposed method, given that in most real cases we have insufficient prior information about the deformation over the area of interest.

After networking the coherent points using local Delaunay [17], the wrapped phase differences at arcs are obtained and the observation function is then formed. As expected, the determinant of the coefficient matrix is close to zero indicating the observation function is ill-posed. By applying the ridge estimator with phase ambiguity detection and integrating the parameters at arcs to points, the deformation time series are finally retrieved as shown in Fig. 6. We then calculate the deformation rate from the time series and compare with the input deformation signal. The discrepancy has a mean of 0.02 mm/year with a standard deviation of 0.93 mm/year. This illustrates that the proposed method can effectively estimate ground deformation from wrapped interferograms without including the DEM residual as a parameter.

Considering the combination methodology can possibly enlarge the atmospheric artifacts in pseudo-interferograms, we further evaluate this effect on the parameter estimation under a scenario where radar signals over 30% areas in 50% acquisitions are assumed to be randomly delayed by atmosphere with a maximum magnitude of 1.5 rad. Fig. 7 shows the difference between absolute atmospheric phases at arcs (i.e.,$|\phi^{\text{pseudo}}_{\text{arc,aps}}| - |\phi^{\text{ori}}_{\text{arc,aps}}|$), where $|\emptyset^{\text{ori}}_{\text{arc,aps}}|$ corresponds to the mean value of absolute phases from 27 original interferograms, while $|\emptyset^{\text{pseudo}}_{\text{arc,aps}}|$ represents the mean value of absolute phases from 23 pseudo-interferograms. It indicates that as observations of MTInSAR model, the phase differences at arcs are less affected by atmospheric artifacts and the combination does not necessarily always enlarge the atmospheric components at arcs. Since the mean of difference is around 0.05 rad, it is safe to conclude that deformation rates estimated from combined interferograms would not be significantly impacted by the enlargement of atmospheric artifacts. It is also worth noting that spatial differential operation can reduce the atmospheric artifacts, though not eliminate it completely. Once the deformation time series is obtained, further processing (e.g., filtering [13] and principal component analysis [37]) is usually compulsory for the removal of any remaining atmospheric component.

We next apply the proposed method on a set of TerraSAR-X data available over an urbanized area in Tianjin, China (Fig. 8). A total of 22 images were acquired from 20090828 to 20100427 from which 48 interferograms are generated with maximum baselines of 33 d and 227 m. We then construct pseudo interferograms by integer combination, whose maximum perpendicular baseline has been shortened to 2 m. The combination matrix used can be found in Fig. 9. A set of combined interferograms are shown in Fig. 10. As expected, the topographic phases have been considerably reduced. From these pseudo interferograms, we select 137 752 coherent points, construct 445 925 arcs, and build the observation model between the phase differences and interval deformation rates. To check the condition of the normal matrix, we calculate its determinant. The value of 1.21e-75 indicates a strong correlation among the existing interval parameters, which leads to an ill-posed observation model. From the L-curve, we determine the value of 0.4 as the regularization factor and then conduct ridge estimation with the phase ambiguity detector where 1.2 rad is set to distinguish those arcs whose observations have nonzero integers. Fig. 11 shows the deformation time series retrieved from these pseudo interferograms. It indicates the accumulated deformation along the line-of-sight (LOS) direction in the half-year acquisition period is up to 72 mm, which is consistent with the results reported in [37] and [38].

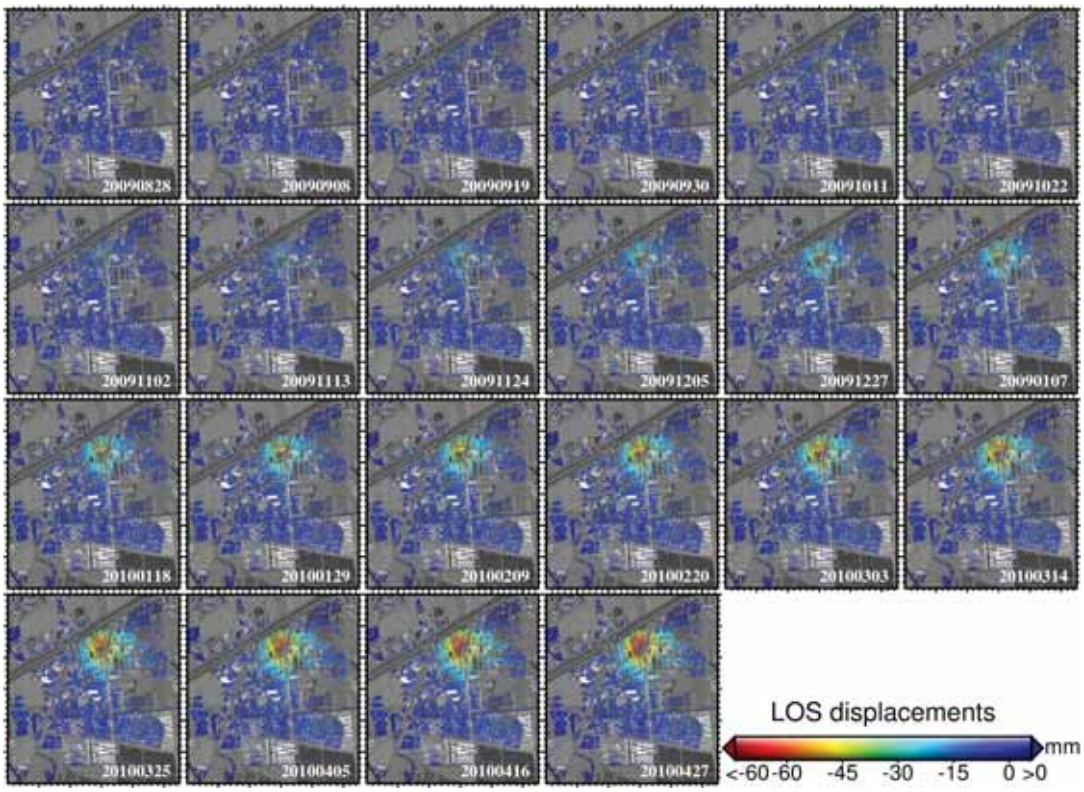

Fig. 11. Deformation time series over an area of Tianjin, China, retrieved from pseudo-interferograms with ridge estimation. The reference point was arbitrarily selected.

IV. Conclusion

Since InSAR measures the phase difference along the LOS direction, any factor that can alter LOS distance would become a component of the InSAR phase measurement. Among these factors, deformation and topographic height are usually dominant. Accurate separation of those has long been an important though challenging issue; current processing methods, including differential with external DEMs and popular MTInSAR estimators, have proven to be inadequate. We have proposed here an alternative strategy capable of minimizing the effect of height on deformation retrieval, therefore making the height estimation unnecessary. The strategy is rooted in the fact that interferograms are the linear combination of SLC images and a further combination of wrapped interferograms with integers can alter the ambiguity density. Via integer combination, we can generate sufficient pseudo-interferograms with ultrashort baselines in which the topographic component is negligible. When taking these interferograms as observations, the pursued deformation turns out to be the only signal that should be parametrized. We have demonstrated the feasibility of retrieving deformation time series with the proposed strategy where regularization is compulsory to deal with the ill-posed coefficient matrix raised by the correlation among the parameters. It is worth noting that the proposed strategy can also be used to just retrieve the deformation rate over the whole time span. In this case, since the rate is the only and single parameter in the model, an extra constraint is no longer needed. As a final remark, although we can mitigate the effects of DEM residuals on deformation retrieval, the height information that is vital for positioning the coherent targets cannot be obtained by the proposed method; in real applications, we are concerned not only with the magnitude of deformations but also with their locations. Accurate elevation model reconstruction from high-resolution SAR data, especially over urban areas, is one of our ongoing research efforts, where the baseline optimization, phase ambiguity, and systematic error raised by improper deformation model will be particularly addressed.

Acknowledgment

The authors would like to thank the German Aerospace Center (DLR) for providing the TerraSAR-X Data via Project MTH1726. They would also like to thank the associate editor and the five anonymous reviewers for their constructive suggestions.

References

[1] A. K. Gabriel, R. M. Goldstein, and H. A. Zebker, "Mapping small elevation changes over large areas: Differential interferometry," *J. Geophys. Res.*, vol. 94, no. B7, pp. 9183–9191, 1989.

[2] D. Massonnet *et al.*, "The displacement field of the Landers earthquake mapped by radar interferometry," *Nature*, vol. 364, no. 6433, pp. 138–142, Jul. 1993.

[3] G. Peltzer and P. Rosen, "Surface displacement of the 17 May 1993 Eureka Valley, California, earthquake observed by SAR interferometry," *Science*, vol. 268, no. 5215, pp. 1333–1336, Jun. 1995.

[4] A. Moreira, P. Prats–Iraola, M. Younis, G. Krieger, I. Hajnsek, and K. P. Papathanassiou, "A tutorial on synthetic aperture radar," *IEEE Geosci. Remote Sens. Mag.*, vol. 1, no. 1, pp. 6–43, Mar. 2013.

[5] Z. Lu and D. Dzurisin, *InSAR Imaging of Aleutian Volcanoes: Monitoring a Volcanic Arc from Space*. Berlin, Germany: Springer, 2014.

[6] J. Dong *et al.*, "Mapping landslide surface displacements with time series SAR interferometry by combining persistent and distributed scatterers: A case study of Jiaju landslide in Danba, China," *Remote Sens. Environ.*, vol. 205, pp. 180–198, Feb. 2018.

[7] L. N. Schaefer, F. Di Traglia, E. Chaussard, Z. Lu, T. Nolesini, and N. Casagli, "Monitoring volcano slope instability with synthetic aperture radar: A review and new data from Pacaya (Guatemala) and Stromboli (Italy) volcanoes," *Earth Sci. Rev.*, vol. 192, pp. 236–257, May 2019.

[8] A. Moreira *et al.*, "Tandem-L: A highly innovative bistatic SAR mission for global observation of dynamic processes on the earth's surface," *IEEE Geosci. Remote Sens. Mag.*, vol. 3, no. 2, pp. 8–23, Jun. 2015.

[9] H. A. Zebker and P. Rosen, R. M. Goldstein, A. Gabriel, and C. L. Werner "On the derivation of coseismic displacement fields using differential radar interferometry: The Landers earthquake," *J. Geophys. Res.*, vol. 99, no. B10, pp. 19617–19634, Oct. 1994.

[10] M. Werner, "Shuttle radar topography mission (SRTM) mission overview," *Frequenz*, vol. 55, no. 3, pp. 75–79, Mar. 2001.

[11] K. J. Bhang, F. W. Schwartz, and A. Braun, "Verification of the vertical error in C-band SRTM DEM using ICESat and Landsat-7, Otter Tail County, MN," *IEEE Trans. Geosci. Remote Sens.*, vol. 45, no. 1, pp. 36–44, Jan. 2007.

[12] A. Gruber, B. Wessel, M. Huber, and A. Roth, "Operational TanDEM-X DEM calibration and first validation results," *ISPRS J. Photogramm. Remote Sens.*, vol. 73, pp. 39–49, Sep. 2012.

[13] A. Ferretti, C. Prati, and F. Rocca, "Permanent scatterers in SAR interferometry," *IEEE Trans. Geosci. Remote Sens.*, vol. 39, no. 1, pp. 8–20, Jan. 2001.

[14] P. Berardino, G. Fornaro, R. Lanari, and E. Sansosti, "A new algorithm for surface deformation monitoring based on small baseline differential SAR interferograms," *IEEE Trans. Geosci. Remote Sens.*, vol. 40, no. 11, pp. 2375–2383, Nov. 2002.

[15] S. V. Samsonov and N. D'Oreye, "Multidimensional small baseline subset (MSBAS) for two-dimensional deformation analysis: Case study Mexico City," *Can. J. Remote Sens.*, vol. 43, no. 4, pp. 318–329, Jul. 2017.

[16] O. Mora, J. J. Mallorqui, and A. Broquetas, "Linear and nonlinear terrain deformation maps from a reduced set of interferometric SAR images," *IEEE Trans. Geosci. Remote Sens.*, vol. 41, no. 10, pp. 2243–2253, Oct. 2003.

[17] L. Zhang, X. Ding, and Z. Lu, "Modeling PSInSAR time series without phase unwrapping," *IEEE Trans. Geosci. Remote Sens.*, vol. 49, no. 1, pp. 547–556, Jan. 2011.

[18] L. Zhang, Z. Lu, X. Ding, H.-S. Jung, G. Feng, and C.-W. Lee, "Mapping ground surface deformation using temporarily coherent point SAR interferometry: Application to Los Angeles Basin," *Remote Sens. Environ.*, vol. 117, pp. 429–439, Feb. 2012.

[19] G. Fornaro, S. Verde, D. Reale, and A. Pauciullo, "CAESAR: An approach based on covariance matrix decomposition to improve multibaseline–multitemporal interferometric SAR processing," *IEEE Trans. Geosci. Remote Sens.*, vol. 53, no. 4, pp. 2050–2065, Apr. 2015.

[20] G. Ferraioli, C.-A. Deledalle, L. Denis, and F. Tupin, "Parisar: Patch-based estimation and regularized inversion for multibaseline SAR interferometry," *IEEE Trans. Geosci. Remote Sens.*, vol. 56, no. 3, pp. 1626–1636, Mar. 2018.

[21] Y. Du, L. Zhang, G. Feng, Z. Lu, and Q. Sun, "On the accuracy of topographic residuals retrieved by MTInSAR," *IEEE Trans. Geosci. Remote Sens.*, vol. 55, no. 2, pp. 1053–1065, Feb. 2017.

[22] B. Bayer, D. Schmidt, and A. Simoni, "The influence of external digital elevation models on PS-InSAR and SBAS results: Implications for the analysis of deformation signals caused by slow moving landslides in the northern apennines (Italy)," *IEEE Trans. Geosci. Remote Sens.*, vol. 55, no. 5, pp. 2618–2631, May 2017.

[23] Y. T. Yoon, M. Eineder, N. Yague-Martinez, and O. Montenbruck, "TerraSAR-X precise trajectory estimation and quality assessment," *IEEE Trans. Geosci. Remote Sens.*, vol. 47, no. 6, pp. 1859–1868, Jun. 2009.

[24] R. Torres *et al.*, "GMES Sentinel-1 mission," *Remote Sens. Environ.*, vol. 120, pp. 9–24, May 2012.

[25] W. Xu, E. C. Chang, L. K. Kwoh, H. Lim, A. Heng, and W. Cheng, "Phase-unwrapping of SAR interferogram with multi-frequency or multi-baseline," in *Proc. IEEE Int. Geosci. Remote Sens. Symp.*, Pasadena, CA, USA, Aug. 1994, pp. 730–732.

[26] D. Massonnet, H. Vadon, and M. Rossi, "Reduction of the need for phase unwrapping in radar interferometry," *IEEE Trans. Geosci. Remote Sens.*, vol. 34, no. 2, pp. 489–497, Mar. 1996.

[27] U. Wegmüller, M. Santoro, C. Werner, T. Strozzi, A. Wiesmann, and W. Lengert, "DEM generation using ERS–ENVISAT interferometry," *J. Appl. Geophys.*, vol. 69, no. 1, pp. 51–58, Sep. 2009.

[28] R. F. Hanssen, *Radar Interferometry: Data Interpretation and Error Analysis*. Dordrecht, The Netherlands: Kluwer, 2001.

[29] P. S. Agram and M. Simons, "A noise model for InSAR time series," *J. Geophys. Res. Solid Earth*, vol. 120, no. 4, pp. 2752–2771, Mar. 2015.

[30] S. Samsonov, "Topographic correction for ALOS PALSAR interferometry," *IEEE Trans. Geosci. Remote Sens.*, vol. 48, no. 7, pp. 3020–3027, Jul. 2010.

[31] H. Fattahi and F. Amelung, "DEM error correction in InSAR time series," *IEEE Trans. Geosci. Remote Sens.*, vol. 51, no. 7, pp. 4249–4259, Jul. 2013.

[32] A. N. Tikhonov, "Regularization of incorrectly posed problems," *Soviet Math. Doklady*, vol. 4, no. 6, pp. 1624–1627, 1963.

[33] A. N. Tikhonov and V. A. Arsenin, *Solutions of Ill-posed problems*. Washington, DC, USA: Winston, 1977.

[34] P. C. Hansen, "Analysis of discrete ill-posed problems by means of the L-curve," *SIAM Rev.*, vol. 34, no. 4, pp. 561–580, Dec. 1992.

[35] M. Costantini, S. Falco, F. Malvarosa, F. Minati, F. Trillo, and F. Vecchioli, "Persistent scatterer pair interferometry: Approach and application to COSMO-SkyMed SAR data," *IEEE J. Sel. Topics Appl. Earth Observ. Remote Sens.*, vol. 7, no. 7, pp. 2869–2879, Jul. 2014.

[36] M. Costantini, F. Malvarosa, and F. Minati, "A general formulation for redundant integration of finite differences and phase unwrapping on a sparse multidimensional domain," *IEEE Trans. Geosci. Remote Sens.*, vol. 50, no. 3, pp. 758–768, Mar. 2012.

[37] Y.-N. N. Lin, A. Kositsky, and J.-P. Avouac, "PCAIM joint inversion of InSAR and ground-based geodetic time series: Application to monitoring magmatic inflation beneath the Long Valley Caldera," *Geophys. Res. Lett.*, vol. 37, no. 23, Dec. 2010, Art. no. L23301.

[38] Q. Luo, D. Perissin, H. Lin, Y. Zhang, and W. Wang, "Subsidence monitoring of Tianjin suburbs by TerraSAR-X persistent scatterers interferometry," *IEEE J. Sel. Topics Appl. Earth Observat. Remote Sens.*, vol. 7, no. 5, pp. 1642–1650, May 2014.

[39] X. Qin, M. Liao, L. Zhang, and M. Yang, "Structural health and stability assessment of high-speed railways via thermal dilation mapping with time-series InSAR analysis," *IEEE J. Sel. Topics Appl. Earth Observ. Remote Sens.*, vol. 10, no. 6, pp. 2999–3010, Jun. 2017.

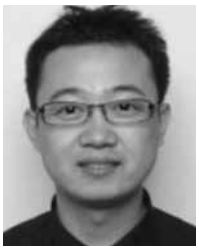

Lei Zhang (S'08–M'11–SM'18) was born in Yantai, China, in 1981. He received the M.Sc. degree from Tongji University, Shanghai, China, in 2007, with a thesis on fault slip inversion with interferometric synthetic aperture radar (InSAR) and GPS data based on a triangular dislocation model, and the Ph.D. degree in geodesy and geodynamics from The Hong Kong Polytechnic University, Hong Kong, in 2011.

From 2012 to 2018, he was a Research Assistant Professor (RAP) with the Department of Land Surveying and Geo-Informatics, The Hong Kong Polytechnic University. Since 2019, he has been a RAP with the Faculty of Architecture, The University of Hong Kong. His research interests include developing advanced processing techniques for SAR data and the application of multi-temporal interferometric analysis on the retrieval of urban morphology, ground displacement, and geophysical parameters, with an emphasis on natural/metrological hazard monitoring and mitigation.

Hongguo Jia received the bachelor's degree in planning and management of resource and environment from Wuhan University, Wuhan, China, the master's degree in surveying from the University of Applied Sciences in Stuttgart, Stuttgart, Germany, and the Ph.D. degree in remote sensing from the Southwest Jiaotong University, Chengdu, China.

She is currently an Assistant Professor with the Faculty of Geosciences and Environmental Engineering, Southwest Jiaotong University. Her research interests include radar interferometry and photogrammetry.

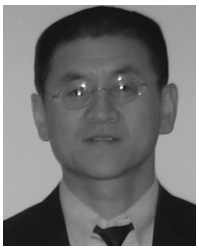

Zhong Lu received the B.S. and M.S. degrees from Peking University, Beijing, China, in 1989 and 1992, and the Ph.D. degree from the University of Alaska Fairbanks, Fairbanks, AK, USA, in 1996.

From 1997 to 2013, he was a Physical Scientist with United States Geological Survey. He is currently a Professor and the Endowed Shuler-Foscue Chair with the Roy M. Huffington Department of Earth Sciences, Southern Methodist University, Dallas, TX, USA. He has authored or coauthored more than 180 peer-reviewed journal articles and book chapters focused on InSAR techniques and applications, and a book on *InSAR Imaging of Aleutian Volcanoes: Monitoring a Volcanic Arc from Space* (Springer, 2014). His research interests include technique developments of interferometric synthetic aperture radar (InSAR) processing and their applications to the study of volcano, landslide, and coastal processes among others.

Dr. Lu is a member of NASA-India SAR (NISAR) Science Team since 2012. He is currently a Senior Associate Editor of journal *Remote Sensing* and journal *Frontier in Earth Sciences*, and a member of editorial boards of *International Journal of Image and Data Fusion* and *Geomatics, Natural Hazards and Risk*.

Hongyu Liang (S'18) was born in Bazhong, China, in 1991. He received the B.S. degree from Southwest Jiaotong University, Chengdu, China, in 2013, and the M.Sc. degree in geomatics from The Hong Kong Polytechnic University, Hong Kong, in 2013. He is currently pursuing the Ph.D. degree at the Department of Land Surveying and Geo-Informatics, The Hong Kong Polytechnic University.

His research interests include estimation theory and advanced processing developments for multi-temporal SAR interferometry and deformation monitoring.

Xiaoli Ding received the B.S. degree from Central South University, Changsha, China, in 1983, and the Ph.D. degree from the University of Sydney, Sydney, NSW, Australia, in 1993.

He is currently the Chair Professor of geomatics and the Associate Dean with the Faculty of Construction and Environment, The Hong Kong Polytechnic University, Hong Kong. He has authored more than 300 papers in these research fields. His research interests include developing technologies for studying ground and structural deformation and geohazards, with a current focus being upon spaceborne geodetic technologies such as GPS and interferometric synthetic aperture radar (InSAR).

Dr. Ding is a Fellow of the International Association of Geodesy (IAG). He is currently the President of subcommission 4.4 of IAG on airborne and spaceborne imaging technologies.

Xin Li was born in Tai'an, Shandong, China, in 1990. She received the B.S. degree in geography information science from the Shandong University of Science and Technology, Qingdao, China, in 2012, and the M.S. degree in the geoinformation science from The Chinese University of Hong Kong (CUHK), Hong Kong, in 2013. She is currently pursuing the Ph.D. degree at the Department of Land Surveying and Geo-Informatics, The Hong Kong Polytechnic University, Hong Kong. Her Ph.D. study focuses on atmosphere pollution analysis and prediction using remote sensing.

Her research interests include the atmospheric remote sensing application and spatial-temporal analysis.